

# **CNWRA** A center of excellence in earth sciences and engineering

A Division of Southwest Research Institute  
6220 Culebra Road • San Antonio, Texas, U.S.A. 78228-5166  
(210) 522-5160 • Fax (210) 522-5155

November 17, 2000  
Contract No. NRC-02-97-009

U.S. Nuclear Regulatory Commission  
ATTN: Mrs. Deborah A. DeMarco  
Office of Nuclear Material Safety and Safeguards  
TWFN MS 8A23  
Washington, DC 20555

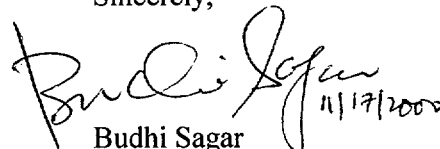
Subject: Transmittal of paper—Application of Integrated Geophysical Techniques to Characterize the Edwards Aquifer, Texas

Dear Mrs. DeMarco:

The enclosed manuscript entitled Application of Integrated Geophysical Techniques to Characterize the Edwards Aquifer, Texas, is based on the work done with a SwRI internal research and development quick-look grant to Dr. Charles Connor of the CNWRA staff. This manuscript is being submitted to the Bulletin of South Texas Geological Society. This work provided an opportunity to utilize geophysical techniques, developed for the NRC's HLW program, on a serious problem in south Texas. The drought over the last several years has seriously stressed the groundwater supply in south Texas. The work described in the accompanying paper demonstrates the potential applicability of geophysics to the better understanding of the recharge and storage of water in the Edwards Aquifer. This paper is being submitted for your information only; no review is requested.

If you have any questions please contact Dr. Charles Connor at (210) 522-6649 or me at (210) 522-5252.

Sincerely,

  
Budhi Sagar  
Technical Director

BS/re  
Enclosure

cc:	J. Greeves	E. Whitt	W. Patrick	S. Sandberg
	J. Holonich	B. Meehan	CNWRA Dirs	W. Downing
	W. Reamer	S. Wastler	CNWRA EMs	T. Nagy
	T. Essig	P. Justus	C. Connor	
	J. Linehan	J. Trapp	R. Green	

D:\GLGP Group\CONNOR\Papers\Bstg-1100\LM111700bs.wpd



Washington Office • Twinbrook Metro Plaza #210  
12300 Twinbrook Parkway • Rockville, Maryland 20852-1606

**APPLICATION OF INTEGRATED GEOPHYSICAL TECHNIQUES TO  
CHARACTERIZE THE EDWARDS AQUIFER, TEXAS**

by

Charles B. Connor<sup>1</sup> and Stewart K. Sandberg<sup>2</sup>

1. Center for Nuclear Waste Regulatory Analyses, Southwest Research Institute, 6220 Culebra Rd, San Antonio, Texas, 78238-5166, USA, [cconnor@swri.org](mailto:cconnor@swri.org)
2. Department of Geological Sciences, University of Southern Maine, [sandberg@usm.maine.edu](mailto:sandberg@usm.maine.edu)

*draft of November 6, 2000*

*to be submitted to the Bulletin of the South Texas Geological Society*

**Abstract**

Integrated geophysical surveys can provide new insights into the geologic structures controlling groundwater flow in the Edwards Aquifer, one of the largest freshwater aquifers in the United States and the sole source of drinking water for the city of San Antonio, Texas. Here, we demonstrate the feasibility of integrated geophysical surveys at a site near two monitoring wells at the western edge of the Knippa Gap, where groundwater flows across the Balcones fault system and downdip into the Maverick Basin. In this area, normal faults controlling groundwater flow are partially obscured by Tertiary sediments, such as the Leona Gravel. Simultaneous inversion of transient

electromagnetic (TEM) and direct current (DC) resistivity data picks the major stratigraphic boundaries, including the top of the Austin Chalk and the top of the Edwards Aquifer itself, at a depth of 237 m (780 ft). These results are in excellent agreement with gamma and lithology logs from the two wells located at the survey site. Large-loop (100-m-side; 324-ft-side) TEM profiling successfully delineates normal faults in the section, in excellent agreement with faults modeled from ground magnetic data. In total, four normal faults were identified by these surveys. Two of these faults were previously known from well log interpretation and two were previously unknown. In addition, the TEM profiles image these faults in the sedimentary section, to the top of the Edwards Aquifer. Thus, modeling TEM soundings, profiles, DC resistivity soundings, and magnetic data together provides a comprehensive view of the geologic structures influencing groundwater flow in this faulted, compartmentalized aquifer.

## **Introduction**

Geophysical techniques are an important component of effective hydrogeological investigations. Repeatedly, geophysical surveys employing a variety of electrical and electromagnetic methods have been used to successfully map stratigraphy, geologic structure, and depth of the water table in major aquifer systems (e.g., Fitterman and Stewart, 1986; Taylor et al., 1992). These investigations have been carried out at a number of scales and in widely varying environments. A major conclusion drawn from these efforts is that significant detail, comparable to information gathered from well logs, can be obtained without drilling when multiple geophysical techniques are employed in

an integrated fashion (e.g., Raiche et al., 1985; Sandberg and Hall, 1990; Sandberg, 1993; Meju et al., 1999).

Here, we demonstrate the utility of integrated surveys for characterization of the Edwards Aquifer using geophysical data gathered adjacent to two monitoring wells that penetrate the Edwards Aquifer at the western margin of the Maverick Basin, in Uvalde County, Texas (Figure 1). To our knowledge, this is the first application of integrated geophysical techniques to characterization of this aquifer, one of the largest in the United States and the sole source of drinking water for the San Antonio metropolitan area (McCarl et al., 1999).

The survey site is located on the Johnson ranch, east of the Frio River, approximately 12 km (7.5 mi) southeast of the city of Uvalde. This area is at the approximate western margin of the Knippa Gap, where groundwater flows south across the Balcones fault system and eastward, downdip, into the Maverick Basin. The Edwards Aquifer is confined and transitions from freshwater to more saline water in this area (Schultz, 1992; Maclay, 1995; Hovorka et al., 1995). There are two monitoring wells at the site, Wells 3 and 4, separated by approximately 2.2 km (1.4 mi) (Figure 2). This location was chosen for the demonstration project because: (i) there is excellent well control on the stratigraphy; (ii) regional geologic mapping has revealed predominantly ENE-trending faults of the Balcones fault system (Figure 1) that offset the top of the aquifer; and (iii) pump tests at Wells 3 and 4 have indicated reduced hydraulic communication between the wells, suggesting faults may significantly alter flowpaths in this area. Such compartmentalization of groundwater flowpaths by faults is thought to be

typical of this part of the Edwards Aquifer (Maclay, 1995) and makes it vital to understand and map geologic structure at a variety of scales.

Magnetic, transient electromagnetic (TEM), and direct current (DC) resistivity techniques were selected for this integrated survey. Ground magnetics were chosen because of the ability to very rapidly map variations in the depth and thickness of the Cretaceous (approximately 80 million year old) basalt found in this area. Ground magnetics are particularly sensitive to lateral discontinuities in the basalt, produced by offsets across normal faults. TEM and DC resistivity surveys were conducted to provide information about variation in electrical conductivity as a function of depth, which can be correlated directly with the stratigraphic section. We performed electrical soundings using DC resistivity and a variety of TEM sounding geometries, as described in the following. Data from TEM and DC soundings were jointly inverted to reduce uncertainty in the model results. TEM loop-profiling was also done near Wells 3 and 4, enabling us to build a section of apparent resistivity as a function of depth. Combined, these methods provide details of the geologic structure near Wells 3 and 4 that have not been previously recognized.

From the surface, the stratigraphy at Well 3, interpreted using a gamma log, consists of up to 61 m (200 ft) of clay-rich marls and sediments, overlying the Austin Chalk. These sediments obscure faults in this area that influence groundwater flowpaths in the aquifer. The Austin Chalk includes interbedded Cretaceous basalts beginning at a depth of 91 m (300 ft). Wittke and Mack (1993) determined that compositions in the Uvalde basalts range from nephelinite, through alkaline basalts to true phonolites. As is typical of basaltic volcanic fields, volcanic vents mapped in Uvalde County are quite

limited in their areal extent compared to the lavas and related volcanic and volcanoclastic deposits that surround them (Connor and Conway, 2000). Distal deposits are interbedded with sediment of the Austin Chalk throughout a thickness of several hundred feet in Wells 3 and 4. The deposits of these eruptions likely range from true hyaloclastites, as observed in their first appearance in cuttings from Well 3 (c.f., Schminke et al., 1978), to intra-sediment lava flows (e.g., Batiza and White, 2000), that erupted through and within the soft-sediments of the Cretaceous Austin chalk. The basalts carry a high remanent magnetization, making them readily mapped with ground magnetic techniques, and are pervasively altered to chlorite, giving them a high electrical conductivity compared to unaltered basalts. The Eagle Ford, Buda, and Del Rio formations, with a combined thickness of approximately 70 m (230 ft) are moderate to low permeability units underlying the Austin Chalk and overlying the Edwards Aquifer.

From the outset, we suspected that good resistivity contrast between the Edwards Aquifer and the overlying clay-rich units would cause a prominent anomaly in the TEM data sets. Nevertheless, we were also concerned that the clay-rich units would be sufficiently electrically conductive to reduce our ability to resolve deeper, more resistive units. Results of these surveys (Figure 2) are described in the following.

### **Magnetics**

Ground magnetic data were collected along an E-W traverse approximately 400 m (1312 ft) south of Wells 3 and 4 (Figure 2). These data were collected with a cesium-vapor magnetometer interfaced to a global positioning system (GPS) receiver that provides position information with a one-sigma error of 2.5 m (8 ft) (Connor and Connor, 1999).

GPS and magnetic readings were collected at one second intervals along the traverse, with a total of 2,534 readings gathered along the ~3-km-long (1.9 mi) transect.

Large amplitude, comparatively short-wavelength magnetic anomalies occur along the transect (Figure 3). These anomalies are up to 300 nT in amplitude and are attributed to offsets by faults and perhaps lateral variations in flow thickness that occurred at the time of effusion of these units.

These magnetic data were modeled assuming the basalts have normal polarity and carry a remanent magnetization of 1 Amp/m, a typical value for alkalic basalts (Tarling, 1983). Although the basalts are interbedded with the Austin Chalk, the magnetic anomalies were modeled as a single layer, of variable thickness, and displaced by faults along the transect. This interpretation simplifies the geology somewhat and could be significantly revised if paleomagnetic data were available and with the acquisition of additional magnetic profiles. The depth to the top of the basalt unit is established at Wells 3 and 4 by their first appearance in the well cuttings.

As Figure 3 illustrates, the magnetic variation along the profile is readily modeled using these assumptions. The steep magnetic gradients along the profile are best explained by four normal faults. Three of the four faults have apparent east dips; a single fault located west of Well 4 has apparent west dip. Dip and magnitude of throw of the faults are not well constrained by the magnetic data because of uncertainty resulting from assumptions made about the rock magnetic properties.

### Transient Electromagnetics and Direct Current Resistivity

TEM soundings were performed near Wells 3 and 4 using two 300-m-loops (984-ft-loops) and two profiles of 100-m-loops (329-ft-loops) in a central loop configuration (Figure 2). The central loop (or in-loop) TEM sounding configuration consists of a large square transmitting wire with a vertical dipole receiver located at the center. The transmitter waveform consists of a series of positive and negative current pulses, each terminated by a linear ramp. The receiver samples the voltage in a receiver coil, which is the time derivative of the secondary magnetic field (Spies and Frischknecht, 1991). Data obtained from many transmitter cycles are stacked to cancel random noise. For each loop, soundings were collected for currents transmitted at 3 Hz, 7.5 Hz, and 30 Hz, to provide a total range of measurement time from 0.08813 – 6.978 milliseconds.

Time-dependent apparent resistivity was deduced from the time derivative of the magnetic field using the methods of Sandberg (1990). Briefly, this algorithm solves the equation:

$$Z(\sigma, t) = \frac{\sqrt{\pi} \mu a}{2\delta} \times \frac{A_R}{A_T} \sum_{n=0}^{\infty} \frac{(-1)^n}{4^n n! (2n+3)(2n+5)} \times \left[ \frac{1}{\tau'^{n+\frac{3}{2}}} - \frac{1}{\tau^{n+\frac{3}{2}}} \right] \quad (1)$$

for the apparent resistivity,  $\rho_a (= 1/\sigma)$  where

$$\tau' = \frac{t}{\sigma \mu a^2}$$

$$\tau = \frac{t + \delta}{\sigma \mu a^2}$$

The apparent resistivity, derived from inverting equation 1, is referred to as the ramp-derived apparent resistivity. In these expressions,  $Z$  is the mutual impedance (voltage in the receiver coil divided by the current in the transmitter loop),  $\sigma$  is the half-space conductivity,  $t$  is the measurement time,  $\delta$  is the ramp time,  $\mu$  is the magnetic permeability,  $a$  is the equivalent circular transmitter-loop radius,  $A_R$  is the area of the receiver coil, and  $A_T$  is the area of the transmitter loop. Data from a single 100-m-loop sounding along profile B-B' (Figure 2), for transmitted frequencies of 3 Hz, 7.5 Hz and 30 Hz, are shown in Figure 4. Note the excellent overlap of soundings collected at different frequencies, indicating that the ramp solution (equation 1) for apparent resistivity is accurate.

The apparent resistivity expressed as a function of depth, rather than time, is calculated using the method of Meju (1998):

$$D = \sqrt{\frac{3.9 \rho_a t}{2\pi\mu}} \quad (2)$$

where  $D$  is depth in meters for apparent resistivity,  $\rho_a$ , in ohm-m and time,  $t$ , in seconds. Depth sections plotted with apparent resistivity and equation 2 are approximate, and should be linked to true inversions, as described in the following. Note that greater approximate depths correlate with lower frequencies. Apparent resistivity as a function of depth (equation 2) is quite coherent between soundings on profile B-B' (Figure 5a) and

profile C-C' (Figure 5b). Not only are sounding results coherent across frequencies, but the results are also coherent from sounding to sounding along each profile.

Profile B-B' (Figure 5a) reveals low apparent resistivity values, consistent with the presence of clay-rich sediments in both the shallow section and in the Austin Chalk. Contours of equal apparent resistivity have a gentle east dip along the plane of the profile. These dips are quite consistent except between soundings 3 and 4 of profile B-B', suggesting the presence of geologic structure. For example, the 10 and/or 15 ohm-m contour lines can be followed from sounding 5 (Figure 5a) eastward. The linear trend of these contours, down to the east, is displaced between soundings 3 and 4 on profile B-B'. This change in dip suggests at least one fault is located between soundings 3 and 4 that displaces the dipping sedimentary section, thrown down to the west. The model based on the magnetic data (Figure 3) also suggests the presence of a west-dipping normal fault at this location.

Profile C-C' (Figure 5b) also contains low resistivity values and coherent structure in the approximate depth section. Late time resistivities, associated with greater depths, are noisy on this profile, particularly near soundings 1 and 2. This produces ambiguity in the apparent resistivities in the profile, especially at greater approximate depths (correlating to late times [equation 2]). Also, sounding 3 of profile C-C' (Figure 5b) is somewhat noisy at all times, illustrated by the ripple in apparent resistivity as a function of depth seen in this sounding. This pattern, particularly affecting contours at  $D < 100$  m, suggests that the sounding is affected by the metallic casing of nearby Well 3, or some other source, such as a buried pipeline, that was not observed during the survey. Note that the ground magnetic data (Figure 3) are also noisy in this area, supporting the

idea that sounding 3 (profile C-C') results were affected by the well casing, a buried pipeline, or similar "cultural noise". Nonetheless, the general west apparent dip of the resistivity contours is clear on the western portion of profile C-C'. Note the change in dip of the apparent resistivity contours between soundings 2 and 3 on profile C-C', again suggesting the presence of geologic structure. Although displacement of the apparent resistivity contours is not as clear as on profile B-B', the change in dip is consistent in both soundings 1 and 2 on profile C-C'. As on profile B-B', this structure correlates with the occurrence of a fault, in this case dipping east, inferred in the magnetic model.

While the approximate depth - apparent resistivity sections provide an excellent qualitative perspective of geologic structure in these areas, simultaneous inversion of TEM and resistivity data can also provide quantitative information about well-site stratigraphy. We simultaneously inverted the 100- and 300 m-loop soundings with DC resistivity data collected using a Schlumberger array and maximum  $ab/2$  spacing of 100 m, where  $ab$  is the distance between current electrodes. The DC resistivity sounding provides detail of the shallow resistivity structure, and because it is an independent measure of resistivity, allows us to decouple the resistivity from thickness of units, adding uniqueness to the solution (e.g., Raiche et al., 1985; Sandberg, 1993).

Simultaneous inversion of the three data sets (100-m-loop, 300-m-loop, and DC resistivity) was performed using the EINVRT code (Sandberg, 1990; Sandberg and Hall, 1990). EINVRT uses a standard forward solution for 1D, layered earth, where resistivity varies as a function of depth only (Anderson, 1979). An iterative best-fit to all three data sets is achieved using the Jupp-Vozoff algorithm (Jupp and Vozoff, 1975; Raiche et al., 1985).

Inversion for data collected near Well 3 indicates that the 1D model adequately explains variation observed in all three data sets (Figure 6). The 1D model that produces this fit correlates well with independent stratigraphic information from the Well 3 gamma-log (Figure 7). Specifically, the top of the Austin Chalk at a depth of 58m (190 ft) is seen as an increase resistivity at the same depth. An abrupt increase in resistivity at 238m (783 ft) marks the top of the Edwards Aquifer, in agreement with an abrupt transition the gamma-log, marking the base of the Del Rio Clay. Thus the inversion of the DC resistivity and TEM data, performed independently of other information, agrees well with the lithologic and gamma logs for Well 3.

Of note is that the Eagle Ford, Buda, and Del Rio formations are not differentiated from the Austin Chalk by the inversion. These geologic units are lithologically distinct, as evinced by the gamma log anomalies at approximately 167 m (550 ft) and 213 m (700 ft) (Figure 7). However, they do not have distinct electrical resistivity properties. In this area, the formation resistivity of the Austin Chalk – Del Rio Clay section is complex, and varies between 5 and 30 ohm-m (Alvin Schultz, personal communication to C. Connor, 2000). In contrast, the top of the Edwards Aquifer has a distinctly low resistivity compared to the overlying clay-rich units, and is identified by interpretation of the surface geophysical data.

The basalts, so prominent in the magnetic data, are not observed in the electrical sounding. Although basalts normally are very resistive, these units in Well 3 cuttings have pervasive chloritic alteration, likely resulting from their deposition in a shallow marine environment (Fisher and Schmincke, 1984), which increases their conductivity substantially compared to unaltered basalts.

The apparent resistivity values observed in the 100-m-loop data of profile B-B' (Figure 5a) were re-interpreted in light of the results of the simultaneous inversion and comparison with the magnetic data and model (Figure 8). The top of the Edwards Aquifer, as estimated from the inversion and verified by comparison with the well logs, occurs at an apparent resistivity value of approximately 13 ohm-m in the section south of Well 3 (profile B-B'). Using this criterion, the top of the Edwards shallows to approximately 180 m at the west end of profile B-B'. Assuming that all of the offset between soundings 3 and 4 occurs at a single fault, the vertical throw of this fault is on the order of 30 m. Within the two faults blocks in profile B-B', the top of the Edwards formation has an apparent dip to the east of approximately 15 degrees, based on the apparent resistivity contours.

### **Discussion and Conclusions**

Groundwater flow in the Edwards Aquifer is structurally controlled. These structures include faults, such as those delineated in this study, and likely igneous dikes feeding the Uvalde volcanic field, which in some circumstances form effective barriers to groundwater flow (Maclay and Small, 1983; Aloha and Sagar, 1992). Both dike intrusion and deformation have largely ceased in the aquifer, and as a result many of these structures are obscured by Tertiary sediments, such as the Leona Gravel. Under these circumstances, geophysics can play a role in elucidating the structures that affect groundwater flow, and which would be otherwise missed between infrequently spaced wells.

In this study, we demonstrated that integrated resistivity, electromagnetic, and magnetic surveys can effectively delineate geologic structures in a carbonate aquifer, on the scale of hundreds to thousands of feet. The integrated geophysical survey provided insight into geologic structure not previously recognized in well logs alone. Rather than a single fault causing an anomalous hydraulic response between Wells 3 and 4, we identified four faults, each of which may influence groundwater flowpaths. This level of complexity in geologic structure may be the rule rather than the exception in the Knippa Gap of the Edwards Aquifer. As such, geophysical studies can clearly influence the development of a conceptual model of groundwater flow through the Edwards Aquifer and interpretation of groundwater flow simulations predicted based on this conceptual model.

It is notable that field work for this project was accomplished in three days, with a similar level of effort for data processing. Brief, focussed geophysical surveys such as this one are sufficient to identify the essential elements of the stratigraphic section, normally only determined after drilling. Similar surveys at existing and planned well locations in the Edwards Aquifer may significantly improve our interpretations of the data provided by these wells.

Based on the results of this demonstration project, we are confident that integrated geophysical surveys can be used to characterize the confined portion of the Edwards Aquifer by: (i) augmenting stratigraphic interpretation between distantly spaced wells or at proposed well locations, and (ii) mapping geologic structures that influence groundwater flowpaths. In addition, although not explored in this study, groundwater quality can be successfully mapped using TEM at locations where the groundwater

exhibits a marked decrease in electrical resistivity with degradation of water quality. For example, TEM provides one means of delineating the “saline-water line” in south Texas and the relationship between the saline-water line and geologic features. In the unconfined part of the aquifer, integrated geophysical techniques offer the further advantage of being appropriate to delineate and monitor variations in the groundwater table. In these areas, geophysical methods, such as those described in this manuscript, can be employed to delineate differences in head across fault zones, and rates of groundwater infiltration at significant recharge features. Such information may be of significant benefit in hydrologic model design, verification, and successful predictive groundwater management.

*Acknowledgements:* We gratefully acknowledge Mr. Johnson for providing access to his land and for providing important information about the site area. Peter LaFemina provided expert assistance in modeling the ground magnetic data. Noel Rogers (Geophysical Solutions), Mike Smith, David Farrell, Ron Green, Troy Maxwell, Melissa Hill (all at Center for Nuclear Waste Regulatory Analyses [CNWRA]), Steve Johnson and Phil Rykwaldler (both at Edwards Aquifer Authority [EAA]), and Cory Christoferson provided tremendous help in TEM, magnetic, and GPS data collection in the August heat. Steve Johnson, Alvin Schultz, Geary Schindel (EAA), John Waugh and Denise Renaghan (San Antonio Water System) helped with site selection and introduced the problem. Debbie Waiting prepared Figure 1, using GIS data provided by Sue Hovorka (Texas Bureau of Economic Geology). The authors especially thank Ron Green for providing advice and guidance at all stages of this project. Comments by Ron Green, Wesley

Patrick, and Alvin Schultz improved this manuscript. This work was performed at the CNWRA. Funding for this project was provided by Southwest Research Institute, a non-profit research and development organization in San Antonio, Texas.

## **References**

Ahola, M., and B. Sagar, 1992, Regional groundwater modeling in the saturated zone in the vicinity of Yucca Mountain, Nevada, U. S. Nuclear Regulatory Commission report NUREG/CR-5890, 62 pp.

Anderson, W.L., 1979, Numerical integration of related Hankel transforms of order 0 and 1 by adaptive digital filtering, *Geophysics* 44: 1287-1305.

Batiza, R., and J.D.L. White, 2000, Submarine lavas and hyaloclastites, *Encyclopedia of Volcanoes*, Academic Press, New York, 361-381.

Connor, C.B., and F.M. Conway, 2000, Basaltic volcanic fields, *Encyclopedia of Volcanoes*, Academic Press, New York, 331-343.

Connor L.J., and C.B. Connor, 1999, Real-time geophysics using Linux, *Linux Journal*, July, 1999, 58-61. Available at <http://www.linuxjournal.com>.

Fitterman, D.V., and M.T. Stewart, 1986, Transient electromagnetic sounding for groundwater, *Geophysics* 51: 995-1005.

Fisher, R.V., and H.-U. Schmincke, 1984, *Pyroclastic Rocks*, Springer-Verlag, Berlin, 472 pp.

Hovorka, S.D., R.E. Mace, and E.W. Collins, 1995, Regional distribution and permeability in the Edwards Aquifer, Final Report to Edwards Underground Water District, contract number 93-17-FO, Report Number 95-02, 127 pp.

Jupp, D.L.B., and K. Vozoff, 1975, Stable iterative methods for geophysical inversion, *Geophysical Journal of the Royal Astronomical Society*, 42: 957-976.

Maclay, R.W., 1995, Geology and hydrology of the Edwards aquifer in the San Antonio area, Texas, U.S. Geological Survey Water Resources Investigations Report 95-4186, 64 pp.

Maclay, R.W., and T.A. Small, 1983, Hydrostratigraphic subdivisions and fault barriers in the Edwards aquifer, south-central Texas, USA, in W. Back and P.E. LaMoreaux, eds., V.T. Stringfield Symposium, Processes in Karst Hydrology, *Journal of Hydrology* 61: 127-146.

McCarl, B.A., C.R. Dillon, K.O. Keplinger, R.L. Williams, 1999, Limiting pumping in the Edwards Aquifer: An economic investigation of proposals, water markets, and spring flow guarantees, *Water Resources Research* 35: 1257-1268.

Meju, M.A., 1998, A simple method of transient electromagnetic data analysis, *Geophysics* 63: 405-410.

Meju, M.A., S.L. Fontes, M.F.B. Olivera, J.P.R. Lima, E.U. Ulugergerli, and A.A. Carrasquilla, 1999, Regional aquifer mapping using combined VES-TEM-AMT/EMAP methods in the semi-arid region of Parriaiba Basin, Brazil, *Geophysics*, 62: .

Raiche, A.P., D.L.B. Jupp, H. Rutter, and K. Vozoff, 1985, The joint use of coincident loop transient electromagnetic and Schlumberger sounding to resolve layered structures, *Geophysics*, 50: 1618-1627.

Sandberg, S.K., 1990, Microcomputer software for individual or simultaneous inverse modeling of transient electromagnetic, resistivity, and induced polarization soundings, New Jersey Geological Survey Open-File Report OFR90-1, 160 pp.

Sandberg, S.K., 1993, Examples of resolution improvement in geoelectrical soundings applied to groundwater investigations, *Geophysical Prospecting* 41: 207-227.

Sandberg, S.K., and D.W. Hall, 1990, Geophysical investigation of an unconsolidated coastal plain aquifer system and underlying bedrock geology in central New Jersey, in S.H. Ward, ed., *Geotechnical and Environmental Geophysics, Volume II: Environmental*

and Groundwater, Investigations in Geophysics, No. 5, Society of Exploration Geophysicists, 311-320.

Schmincke, H.-U., P.T. Robinson, W. Ohnmacht, and M.F.J. Flower, 1978, Basaltic hyaloclastites from holes 396B, DSDP Leg 46, Internal Research Report of the Deep Sea Drilling Project 46: 341-355.

Schultz, A.L., 1992, Using geophysical logs in the Edwards aquifer to estimate water quality along the freshwater/saline water interface – Uvalde to San Antonio, Texas, Edwards Underground Water District Report 92-03, 42 pp.

Spies, B.R., and F.C. Frischknecht, 1991, Electromagnetic sounding, in M. N. Nabighian (ed.) Electromagnetic Methods in Applied Geophysics, Vol. 2 Application, Part A, Investigations in Geophysics No. 3, Society of Exploration Geophysicists, 285-426.

Tarling, D.H., 1983, Geomagnetism, London, Chapman and Hall.

Taylor, K., M. Widmer, and M. Chelsley, 1992, Use of transient electromagnetic data to define local hydrogeology in an arid alluvial environment, *Geophysics* 57: 343-352.

Wittke, J.H., and L.E. Mack, 1993, OIB-like mantle source for the continental alkaline rocks of the Balcones Province, Texas: Trace-element and isotopic evidence, *Journal of Geology* 101: 333-334.

## FIGURE CAPTIONS

Figure 1. Location of the Johnson Ranch study area, in Uvalde County. Study site is indicated by large arrow. Faults in the ENE-trending Balcones fault system are indicated by heavy lines. Major roads, rivers, and county boundaries are also shown. The Knippa Gap is located in eastern Uvalde county and westernmost Medina County. Map projection is Universal Transverse Mercator, 1927 North American Datum, zone 14.

Figure 2. Location of geophysical surveys. Magnetic survey is shown by heavy black line (A-A'); TEM loops are shown to scale with 100-m-loop profiles labeled B-B', and C-C'. Location of Schlumberger resistivity soundings near wells 3 and 4 are indicated by solid stars. During pump tests at an irrigation well (labeled pump well), drawdown was significant at well 3 and very limited at well 4, suggesting some structural control on groundwater flowpaths. The course of the Frio River is shown by the dash-dot line; topographic contours are shown by thin black lines (10 ft contour interval); dirt roads are shown by thick dashed lines. Map coordinates are in Universal Transverse Mercator, 1927 North American Datum, zone 14.

Figure 3. Magnetic data collected along transect A-A' (Figure 2) and model. A subset of the data set is shown as solid circles; calculated model using the geometry shown is

indicated by solid line. The model geometry shows basalt interbedded in the Austin Chalk by solid black area, offset by normal faults, indicated by arrows showing displacement.

Figure 4. TEM data collected at sounding 1 on profile B-B' (Figures 2 and 5a). Data collected at 30 Hz (open triangles), 7.5 Hz (solid squares), and 3 Hz (solid diamonds) exhibit excellent overlap at sampling times less than 0.1 s. These data are representative of all of the soundings data collected in this study.

Figure 5a. Approximate depth section calculated from TEM soundings along profile B-B' (Figure 2). Apparent resistivity is contoured at 1 ohm-m interval. Note the consistent dip of resistivity contours, except between soundings 3 (438190 E) and 4 (438290 E), where a fault is indicated by the change in dip. A fault at this location (~438250 E) is revealed by the magnetic data also (Figure 3).

Figure 5b. Approximate depth section calculated from TEM soundings along profile C-C' (Figure 2). At shallow depths (< 300 m) resistivity contours dip gently west, except east of sounding 3 (440730 E), suggesting the presence of a fault. A fault is indicated between soundings 2 and 3 by magnetic anomalies near 440900 E (Figure 3). Noise in the section at late times (depths > 300 m (985 ft)) likely results from nearby noise sources, such as fences. A ripple in sounding 3 may show the influence of the Well 3 casing.

Figure 6. Simultaneous inversion of TEM soundings (solid diamonds) and Schlumberger resistivity soundings (open triangles) for soundings south of Well 3. Model fit, resulting from the simultaneous inversion, is shown by the solid lines. The resulting resistivity section is illustrated in Figure 7.

Figure 7. Comparison of the EM model (data fit shown in Figure 6), derived from simultaneous inversion of 100-m-loop and 300-m-loop TEM data and Schlumberger resistivity soundings, with gamma and lithology log from well 3.

Figure 8. The result of integration of the magnetic data sets, and inversion of TEM and resistivity data is a quantitative interpretation of the approximate depth section, indicating the position of the normal fault and top of the Edwards Aquifer (corresponding to 13 ohm-m apparent resistivity).

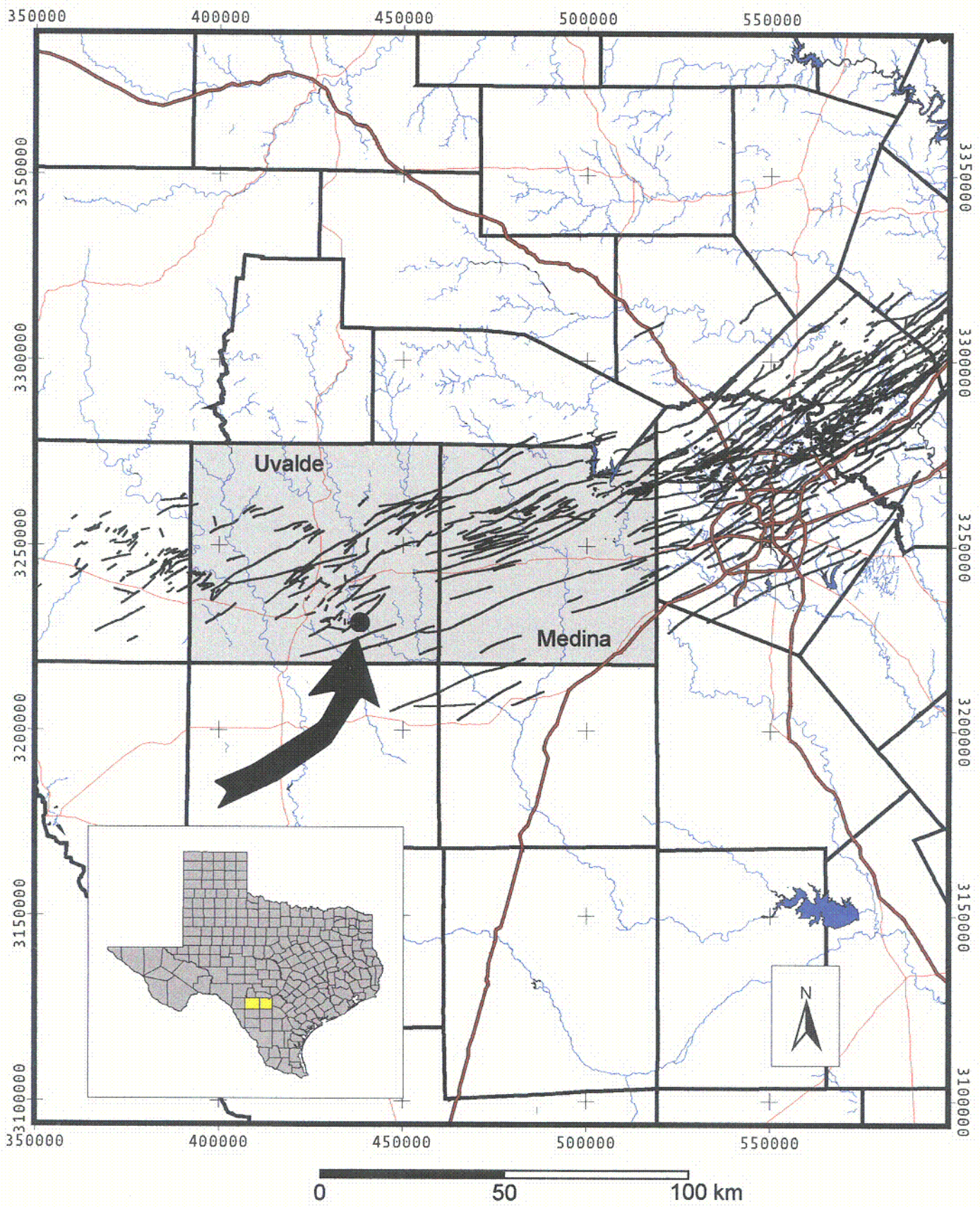


Figure 1.

COI

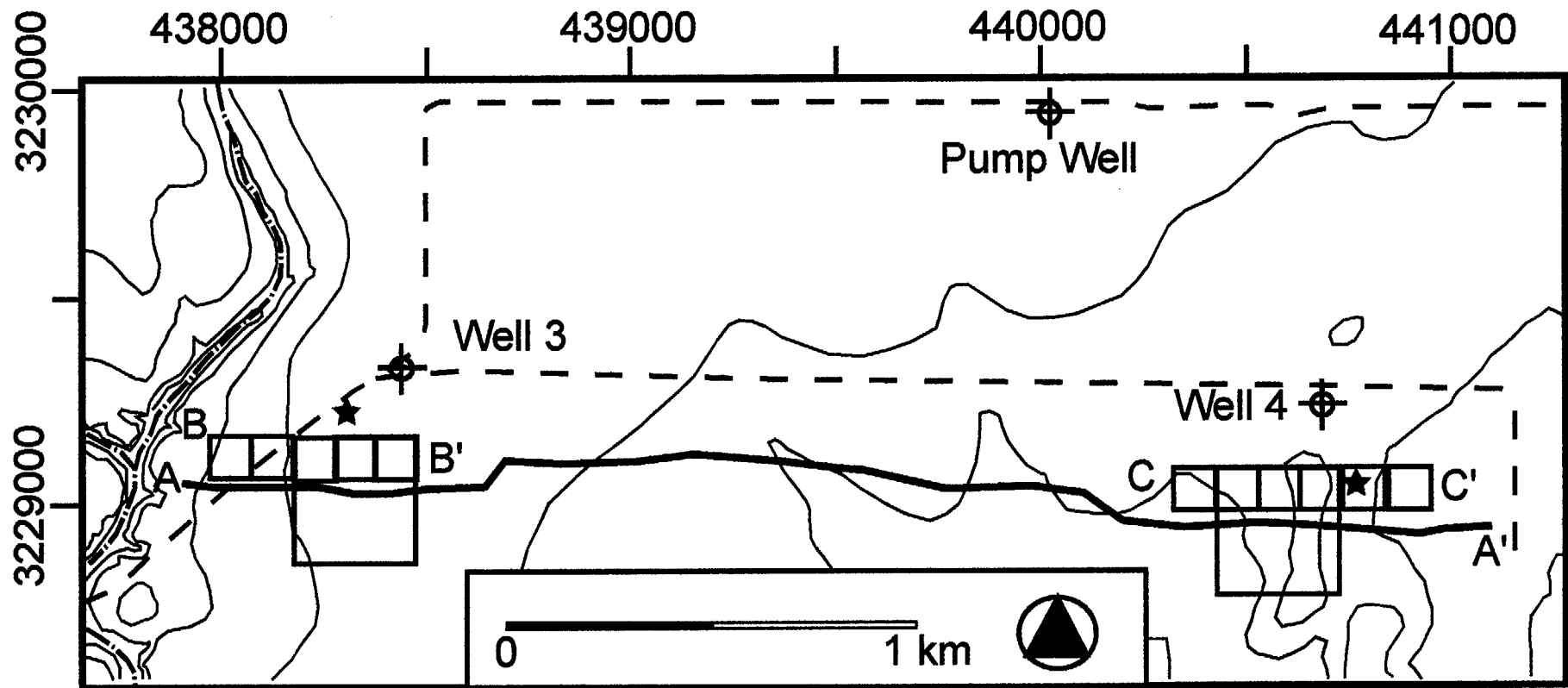


Figure 2.

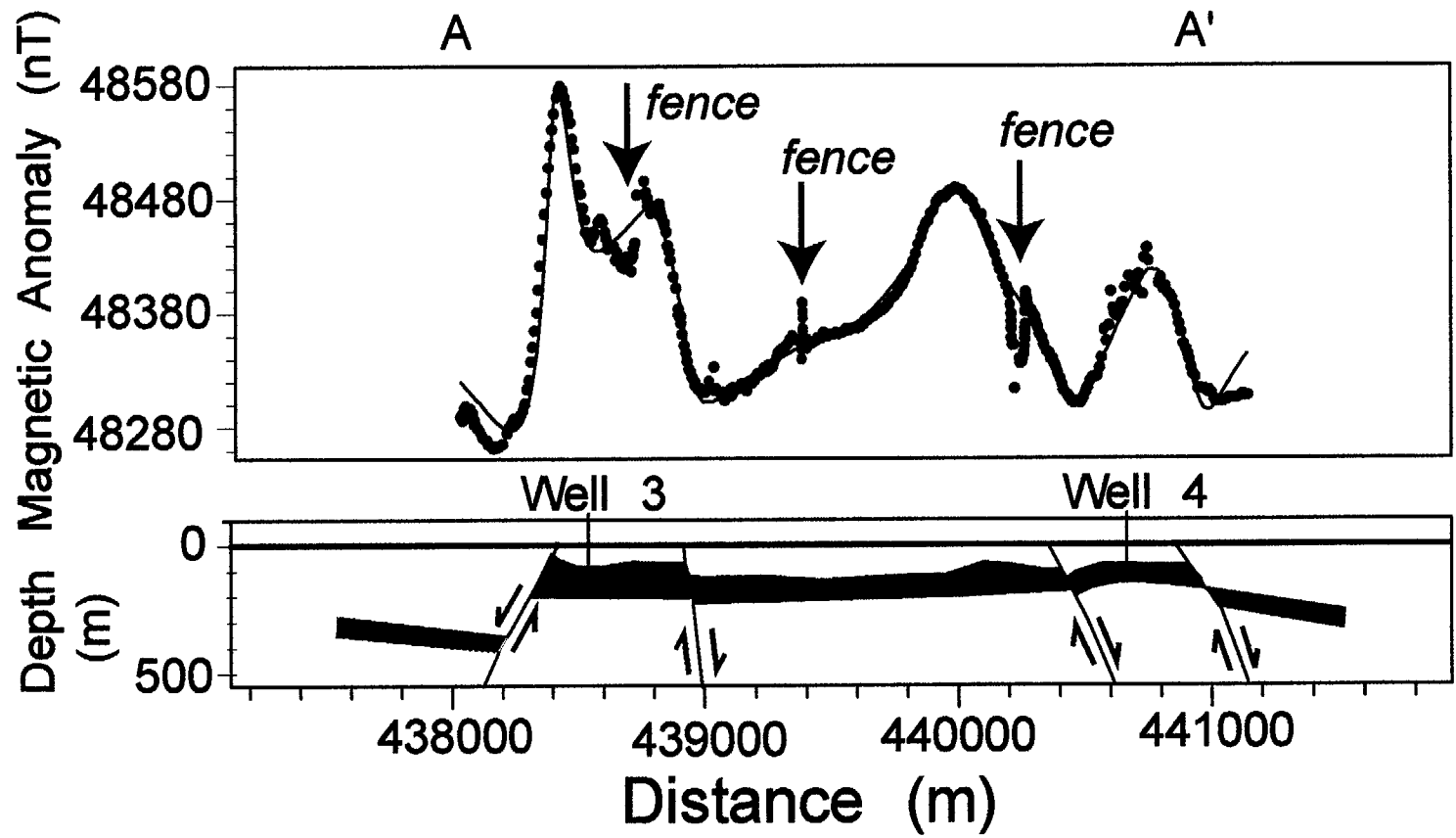


Figure 3.

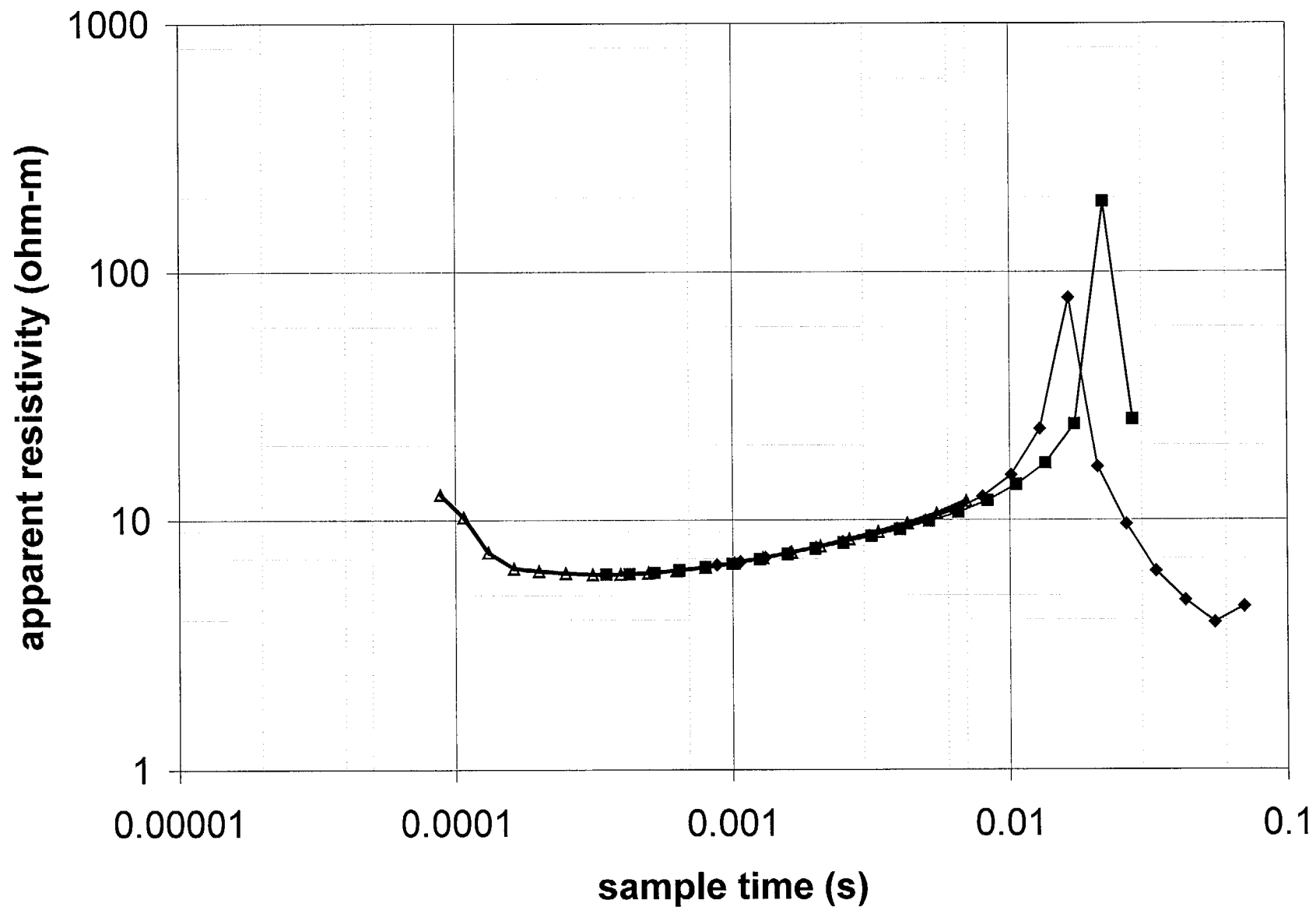


Figure 4.

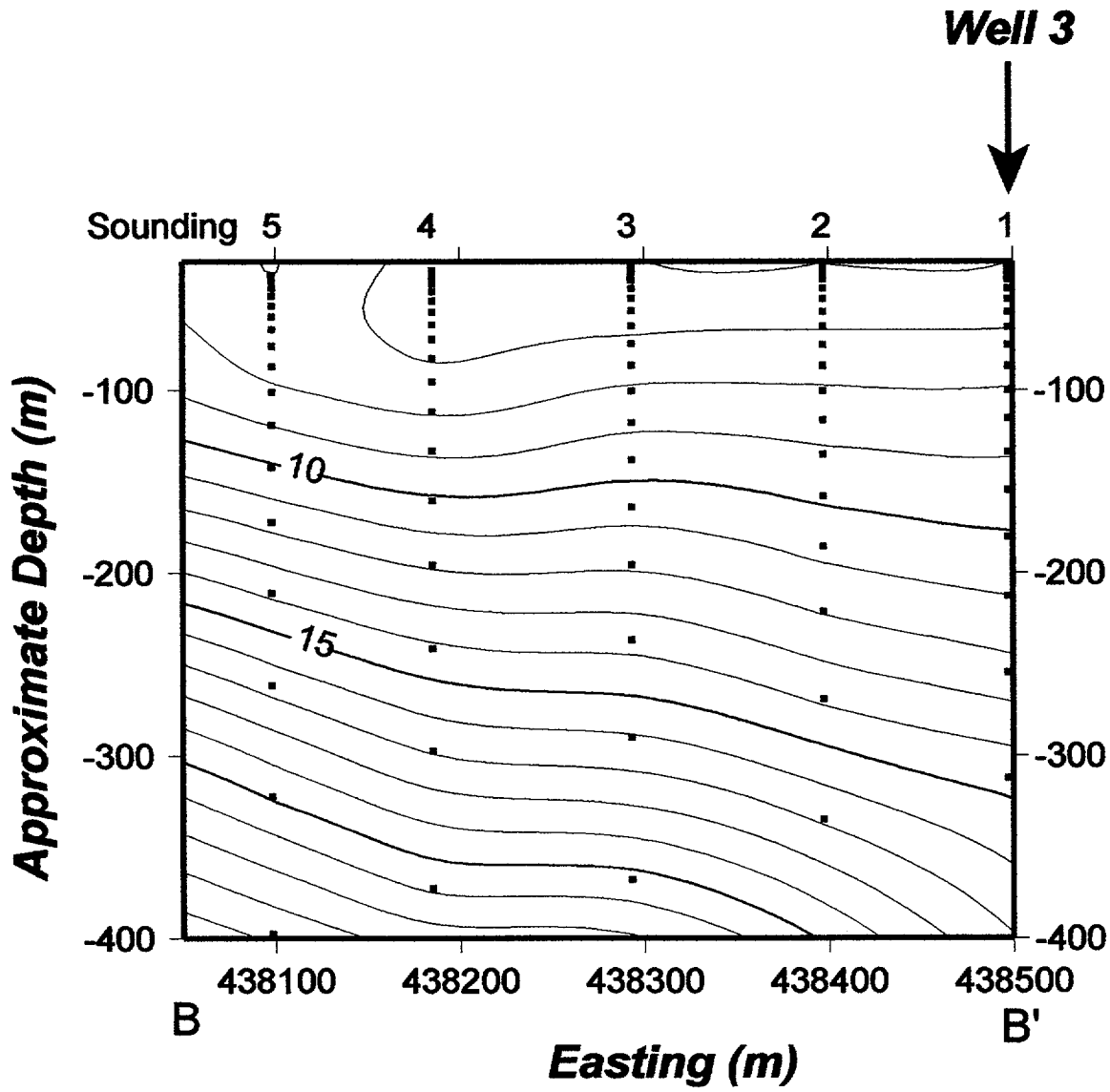


Figure 5a.

**Well 4**



Sounding 6

5

4

3

2

1

**Approximate Depth (m)**

-100

-200

-300

-400

-100

-200

-300

-400

440400

440500

440600

440700

440800

440900

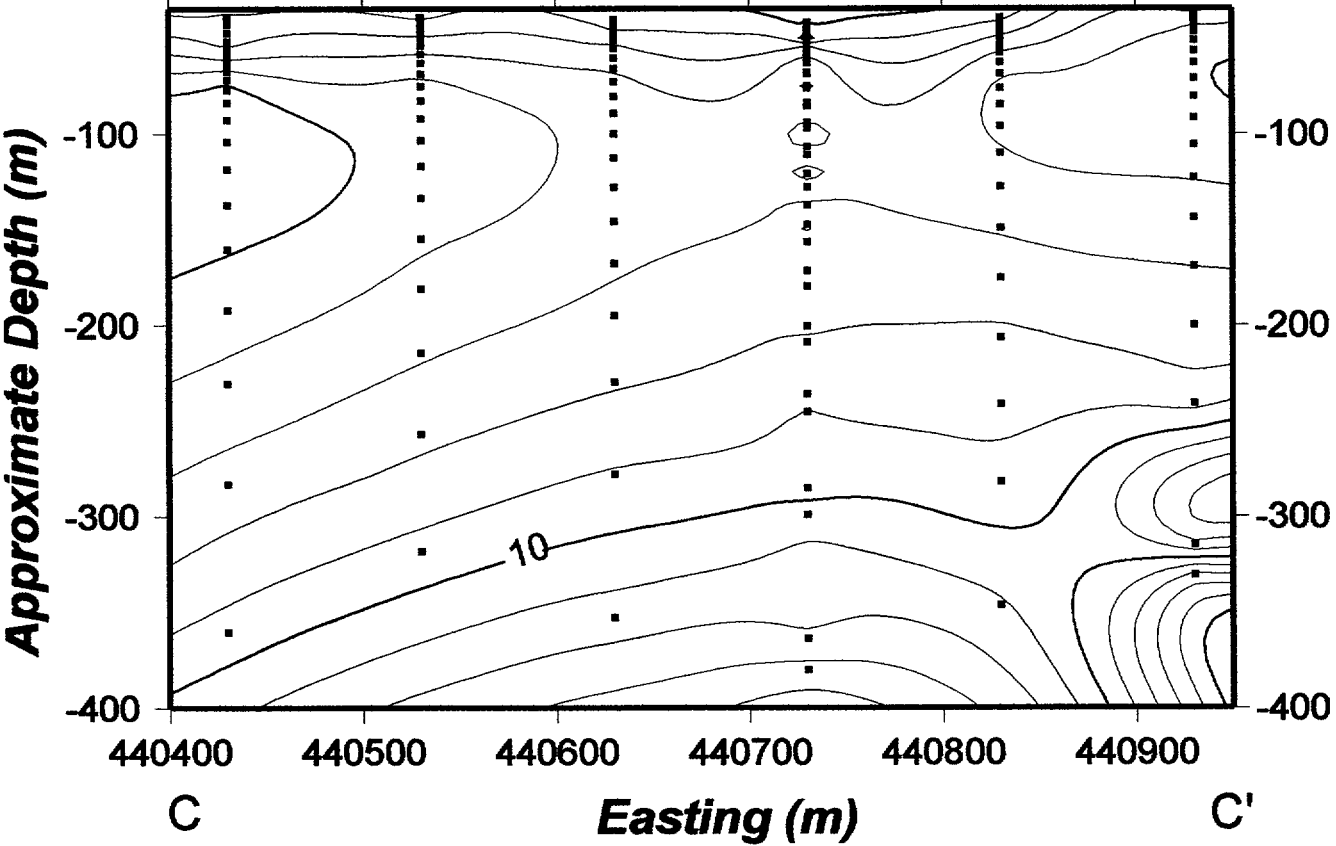
**C**

**Easting (m)**

**C'**

10

Figure 5b.



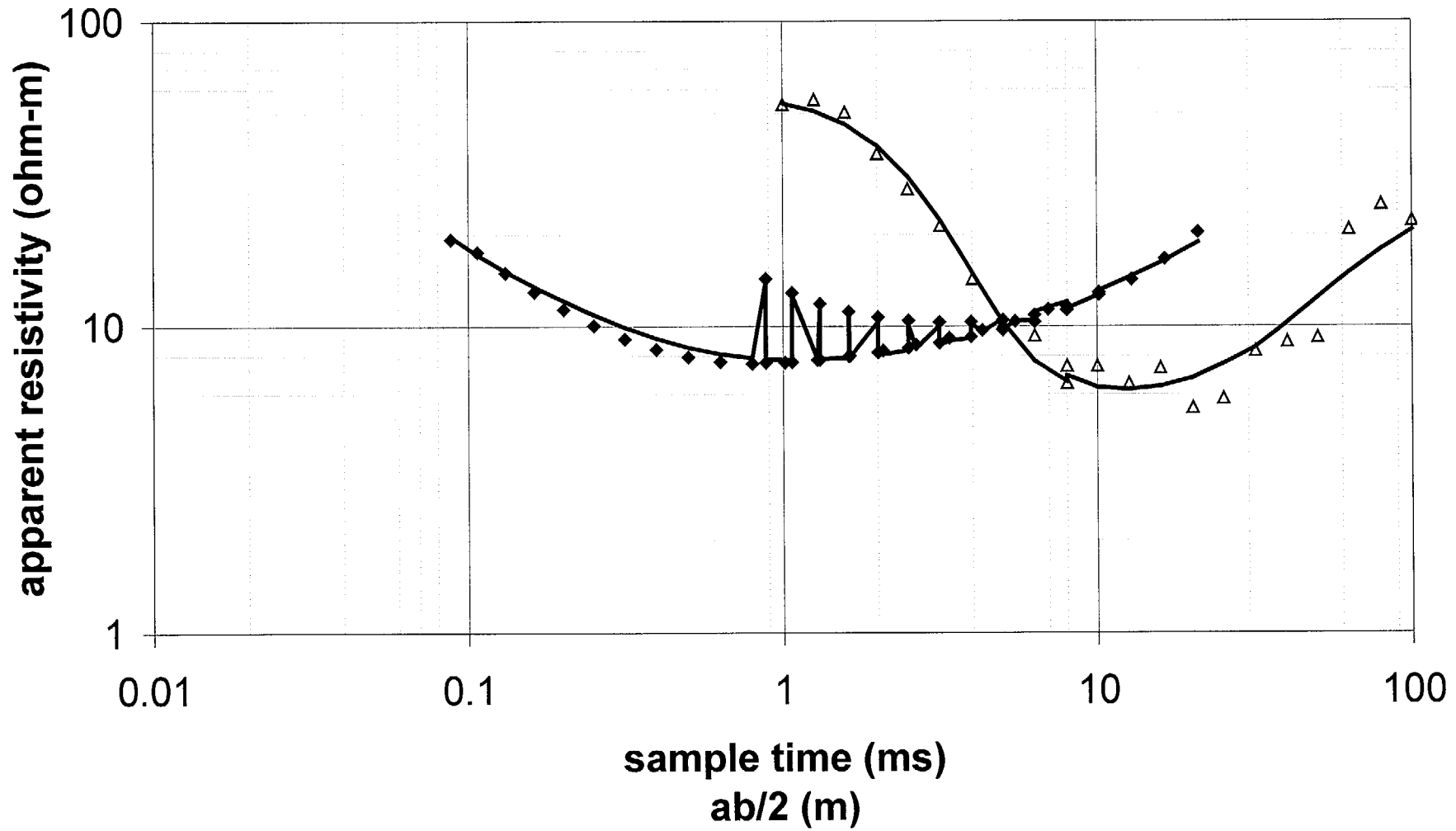


Figure 6.

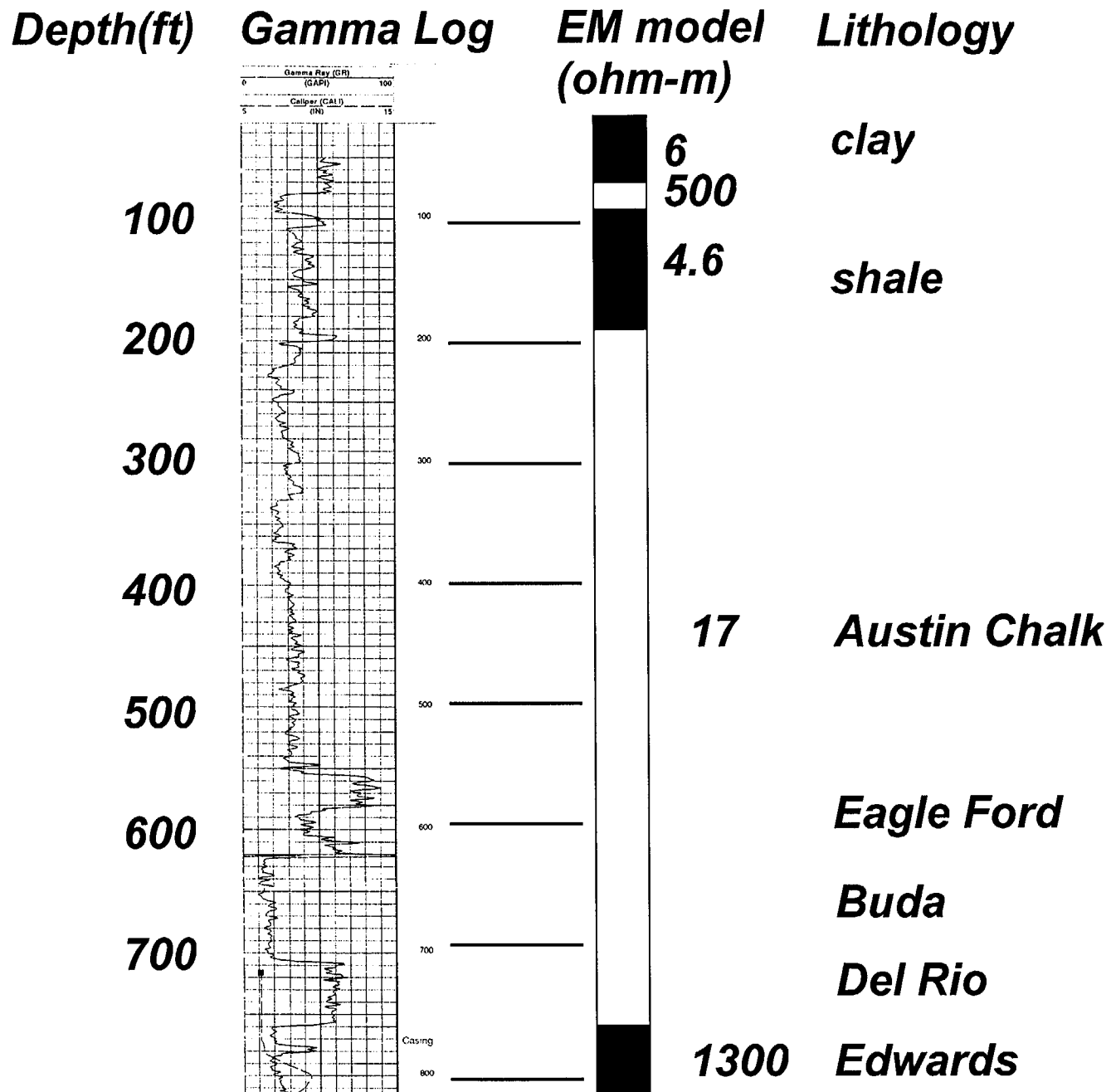


Figure 7.

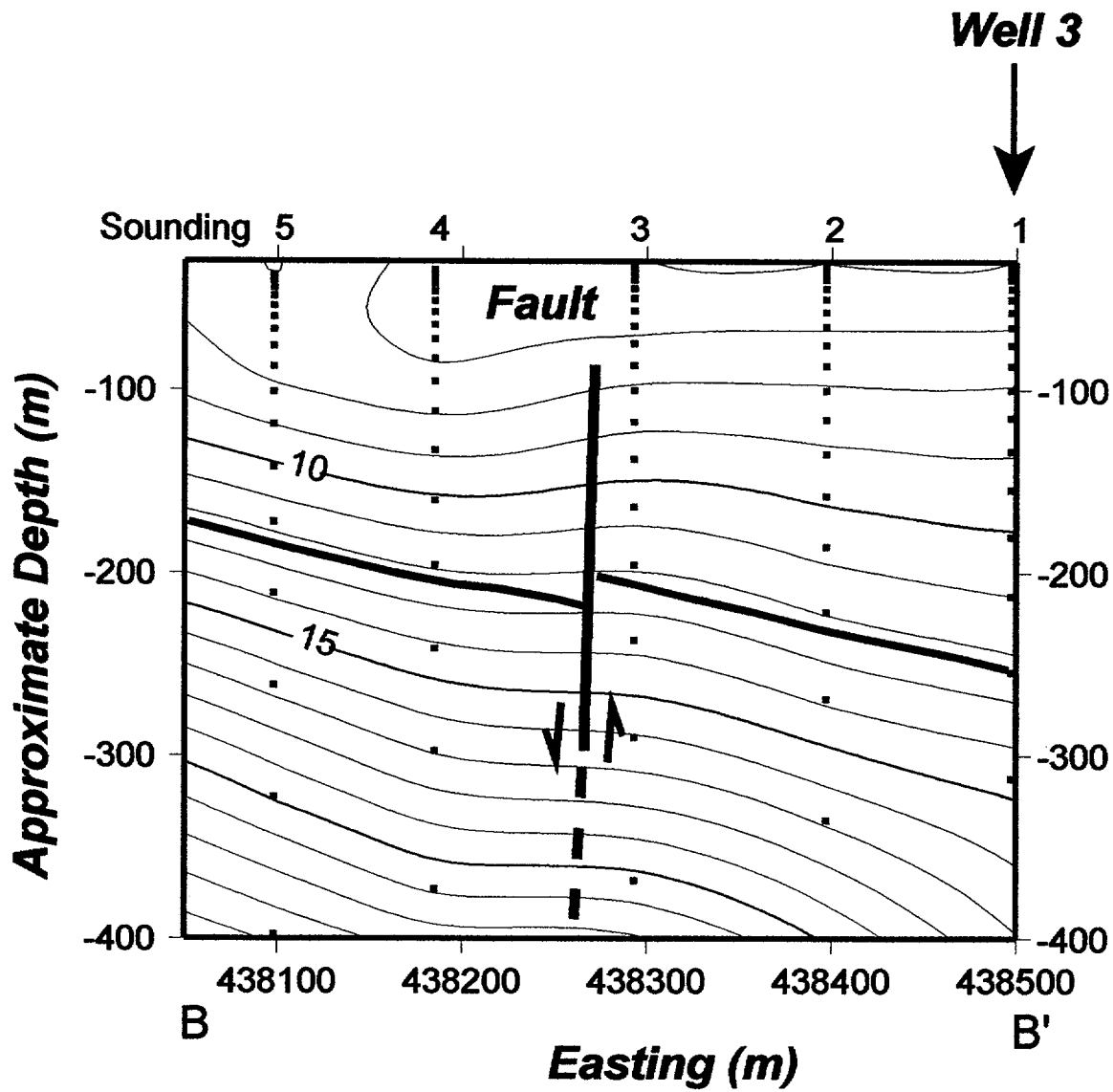


Figure 8.